



New approach of the fouling process modeling in tangential filtration on cake

Bassirou Mahamadou Harouna^a, Othmane Benkortbi^{a,*}, Mabrouk Hamadache^a,
Salah Hanini^a, Abdeltif Amrane^b

^aDepartment of Chemical Engineering and Environment, Faculty of Sciences and Technology, Biomaterials and Transport Phenomena Laboratory (LBMP), Yahia Fares University, Ain d'Heb Medea 26000, Algeria, emails: benkortbi_oth@yahoo.fr (O. Benkortbi), bassymaham@gmail.com (B.M. Harouna), mhamdeche@yahoo.fr (M. Hamadache), s_hanini2000@yahoo.fr (S. Hanini)

^bEcole Nationale Supérieure de Chimie de Rennes, CNRS, UMR 6226, Avenue du Général Leclerc, CS 50837, 35708 Rennes Cedex 7, France, email: abdeltif.amrane@univ-rennes1.fr

Received 23 July 2016; Accepted 10 February 2017

ABSTRACT

This work developed a new theoretical approach for modeling the membrane cross-flow filtration and described the importance of surface energy in the fouling process. In the case of zeta potential membranes, the cake formation results from surface phenomena caused by various interactions at the molecular and the macroscopic level, and is characterized by the surface energy resulting from the action of both gravitational and mechanical forces. The results of the experimental application of the new model revealed that the surface phenomena and the surface forces are the major factors in the fouling process. The new model had undergone various statistical tests to determine its performances and for its comparison with existing models used in wastewater or in drinking water treatment. The considered statistical parameters were the absolute relative error, squared correlation coefficient, the error probability of the experimental points, the distribution function and the correlation coefficient. In this study, two important parameters namely the fouling power Ψ and the overall surface energy γ have been developed; they constituted the contribution of this study in the understanding of the mechanism of membrane fouling. The obtained results showed the impact of the surface interactions, especially at particle wall of the filtering membrane. The level forming the deposit fouling demonstrated that the fouling process from zeta potential membrane is relatively intrinsic from the quantity of surface energy, the characteristic of membrane and the conditions of filtration.

Keywords: Tangential filtration; Membrane fouling; Surface energy; Surface phenomena; Modeling

1. Introduction

The fouling of a filtration membrane is defined by a set of phenomena involved in the modification of its filtration properties. It results from the accumulation of particles on the membrane surface. Its physical, chemical or biological phenomena occurred at the interface, in solution or in the porous volume [1]. The consequence is an obstruction of the pores or the formation of a deposit leading to both changes of permeability and of membrane selectivity [2]. The prediction

of fouling remains a challenge. Fouling mechanisms in a biological membrane process are very complex.

When a membrane system is operated at a constant trans-membrane pressure, the most problematic consequence of fouling is a decrease of the permeate flux with time, which can be extremely accentuated [3,4]. Other direct or indirect effects of fouling are a decrease of the active life of the membranes; thus, more frequent washes are necessary leading therefore to an important consumption of chemical products to compensate the decrease of permeability caused by fouling. It is therefore equivalent to an additional resistance to flow across the membrane [5].

* Corresponding author.

The boundary condition of fluid–porous medium at the interface has been the subject of several studies [6,7]. The classical conditions indicate that the fluid does not slip along the porous wall.

Li et al. [2] developed a fouling model based on the surface phenomena (adsorption). The model also provided a smooth transition from the adsorption regime to the fouling layer filtration regime, based on the flux profiles and the analysis of the membrane surface. Two-step fouling mechanism was proposed to describe the evolution of fouling during continuous cross-flow operation of reverse osmosis membranes.

In their study, Li et al. [6] explained that the standard blocking model fit well with flux data of the original membrane, as well as modified membranes during sodium alginate filtration, indicating that the adsorption fouling was the main reason for flux decline. The slower decrease of the flux rate and the decrease of the adsorption capacity of sodium alginate showed a better anti-fouling property of membranes modified with ZnO. This suggested that a larger repulsive energy should be overcome and a weaker attractive energy for the adsorption of sodium alginate onto the modified membranes surfaces.

A novel pre-treatment method using NO₂ and diethylzinc for further ZnO hydrophilic modification of hydrophobic membranes by atomic layer deposition was examined by Li et al. [7].

The study conducted by Khabthani and El-Asmi [8] showed that the physical phenomena of laminar flow above a porous medium are properly described by the slip conditions, demonstrating that the Darcian rate (U_d) can be neglected when the permeability is quite low.

Modeling of the fouling process has been the subject of several studies following the hydrodynamic and the transport phenomenon due to the importance of this phenomenon in the membrane filtration process.

The numerical implementation of the analytical results obtained allowed the authors to visualize the trajectories of the flow of fluid particles in the three related areas constituted by the half-space semi-infinite bounded on one side by the supposed flat surface of the filter membrane. The first region contains the assumed motor flow governed by the Stokes equations. The second region corresponds to the space in the porous medium where the flow was assumed to be governed by the Darcy equations. The third region consists of a semi-infinite space that is located on the other side of the porous membrane. The work of Hermia [9] dealt with a global description of the fouling steps; they also proposed a model of pores blockage describing linearity between $1/V = f(1/t)$. Schippers and Verdouw [10] studied the cake deposit during filtration and proposed a model of fouling by cake derived from the equations of Darcy and of Shirato et al. [11]. The model is based on the mechanical forces applied both in frontal and tangential filtration.

In their work, Pradhan et al. [12] demonstrated the effect on the filtration performances of the operating conditions, such as filtration flux, air flow rates in terms of ΔP_m , volume of filtered water per unit of membrane area, membrane resistance and particle deposition. The cake resistance was the major resistance contributing to the total membrane resistance.

An almost 60% reduction in particle deposition was observed when the air flow rate was tripled from 600 to 1,800 L/m²·h of membrane area at a flux rate of 15 L/m²·h. Interestingly, the anti-corrosion performance and the mechanical properties of the coating increased remarkably after addition of perfluorodecyltrichlorosilane. Indeed, the observed low adhesion strength, surface energies and the outstanding anti-corrosive properties implied that the obtained coating would be useful in anti-fouling applications [13].

The optimum load of minerals nanoparticles (Al₂O₃) for the fouling mitigation during the activated sludge filtration providing a better understanding of membrane fouling mechanisms. Major findings from this study were polyether-sulfone (PES) membrane characteristics, and performances were changed by the addition of Al₂O₃ nanoparticles to the casting solution, with porosity increasing and the hydrophobic interaction between the membrane surface and foulants decreasing. This fouling solution was proposed by Maximous et al. [14].

Paipuri et al. [15] proposed a new modeling technique for membrane filtration processes. In this method, the fluid flow is governed by the incompressible Navier–Stokes equation, which is solved using a Lattice Boltzmann technique. Cake formation is captured when volume fraction exceeds 0.64 and modeled as a body force in the fluid. The Ornstein–Zernike integral solution, along with the virial equation of state, is used to establish the osmotic compressibility and the diffusion coefficient as a function of the solute concentration.

Geng and Chen [16] proposed a modified ceramic membrane for electrically assisted filtration with anti-fouling property. Anti-fouling tubular Al₂O₃ microfiltration membranes were successfully developed with a Magneli Ti₄O₇ modified inner layer to enhance filtration performance coupled with external electricity. The anti-fouling performance of tubular Ti₄O₇/Al₂O₃ membranes was evaluated through a homemade cross-flow electrically assisted membrane filtration module for the treatment of three typical feed solutions that are known to foul easily, namely oily wastewater, humic acid and bovine serum albumin.

Kumar et al. [17] presented the performance studies of newly formulated polysulfone–bentonite ultrafiltration membrane for the purification of oily produced water, and the results were compared with standard polysulfone–silica membrane. An improved performance of polysulfone–bentonite membranes was obtained with the desired percent rejection over polysulfone–silica membrane.

The modeling of tangential filtration process of a fluid loaded with particles is a topic of major interest in process engineering. Tangential filtration involves three transfer phenomena in a combined manner and depending on the nature of the membrane, organic, mineral or organomineral [18]. To this combination, the characteristics of the physical, physico-chemical, chemical and biological medium to be filtered can be added.

Thus, it appears from several studies that surface phenomenon is a preponderant force in the filtration process and constitutes a key to better understand the fouling mechanism [2]. Surface phenomena represent adsorption within the pores of the membrane (pore blockage by fouling, intermediate blockage and complete blockage) and on the surface of the filtering wall (fouling by cake formation or deposition of various

substances and/or molecules). The purpose of this study is therefore to establish a fouling model that incorporates surface phenomena combined with transport phenomena in a logistic model of filtration on cake with a realistic description of the steps of the fouling process during the ultrafiltration and nanotangential filtration on membranes of PES.

2. Materials and methods

2.1. Materials

Data processed in this work were collected from experiments supervised by Professor Christian Bouchard of Laval University of Canada, Department of Civil Engineering [19]. In addition, the new proposed model was compared with other models available in the literature in order to determine its performance and the variables that characterize the tangential filtration equation on cake and of the fouling process [20]. Data processing was performed with both OriginPro Ver. 8 and Statistica Ver. 12.5193 software. All calculations were done on Excel 2016. Application tests of the proposed model were also carried out on OriginPro Ver. 8 to find the consistency of the model with the database, model accuracy, its performance and adaptability.

2.2. Modeling methods

2.2.1. Theoretical description of the model

The main criterion of the proposed formulation was the consideration of surface phenomena taking place near the membrane and inside the pores along its thickness and length of filtration. The surface energy is a characteristic quantity represented by all the forces involved in the filtration processes and the fouling of the membrane [21] depending on the fluid flow (Reynolds, direction of the cross-flow), the mineralogical nature of the membrane such as mineral membranes (Al_2O_3 , ZrO_2 , TiO_2) and organomineral (PES, polyacrinolyne, polyvinylidene fluoride, polymethylmethacrylate), the friction surface which joins the electric charge [22,23], the transmembrane pressure to plug the surface by adsorption and the polarization concentration [24].

Considering the dynamics of the system associated with the physicochemical characteristics of the membrane, the inertia of the medium to be filtered according to its viscosity leads to a blockage of the pores until complete blockage leading to the formation of a deposit, and hence a concentration polarization of the material on the surface of the membrane [25].

2.2.2. Model of flow filtration

In this formulation, the permeation flux includes three flow characteristics of the filtration process: capillarity, solubilization–diffusion and solubilization–diffusion–capillarity. Thus, the filtration is carried out according to a mechanism in three phases highlighting the progressive surface energy during the filtration cycles until the establishment of the cake [2,21]. Thus, the new model established a logistic growth of cake fouling according to the overall thickness of filtration.

The equations describing the three phases are considered, namely capillarity (Eq. (1)) according to the theory of Kozeny–Carman; solubilization–distribution (Eq. (2)) according to the theory of the reduction of the pore volume assuming to be

proportional to the volume of the filtered solution; and solubilization–diffusion–capillarity (Eq. (3)) according to the works of Maloberti [26] and Kedem and Katchalsky [27].

Three flows are therefore being observed and described by Eqs. (1)–(3). The resultant of which is Eq. (4) by combining Eqs. (1)–(3), according to a mechanism based on the balance of forces acting on the particle near the membrane by neglecting the interactions of inter-particles [1,2]. Each particle is therefore subject to the resultant of several forces that compel to contribute or not to the formation of the cake.

$$J_i = \frac{\varepsilon d^2}{32\mu\tau} \frac{\Delta P_m}{z} \quad (1)$$

$$J_i = -\frac{D_i C_i}{RT} \text{grad}\mu_i = -\frac{D_i C_i}{RT} \left(\frac{\partial\mu_i}{\partial C_i} \text{grad}C_i + V_i \text{grad}P \right) \quad (2)$$

$$J_i = L_{ij}F_i + \sum_{i \neq j} L_{ij}F_j \quad (3)$$

$$J_{ji} = J_j + 2J_i = -\frac{D_j C_j}{RT} \left(\left(\frac{\partial\mu_j}{\partial C_j} \text{grad}C_j + V_j \text{grad}P \right) + \frac{\varepsilon d^2}{32\mu\tau} \frac{\Delta P_m}{z} \right) + L_{ij}F_i + \sum_{i \neq j} L_{ij}F_j \quad (4)$$

Combining the three precedent equations leads to the global flow of logistic growth that can be described by Eq. (4). Assuming that Darcy’s law is applicable, the established overall flow follows Eq. (5):

$$J_p = \frac{\Delta P_m}{\mu(R_m + R_{ctotale})} = \frac{(P_2 - P_1)L + (P_{atm} + \Delta\Pi)x}{\mu x(R_m + R_{ctotale})} \quad (5)$$

2.2.3. Fouling process

In a tangential filtration process, under constant pressure, the development of the layer cake is limited by the ratio of the shear forces and the adhesion mechanisms of the membrane materials [28]. Thus, the presence of surface interactions within the suspension to be filtered modified the character of fouling fluid by varying the reversibility of the accumulated layers. This can result in critical operating conditions. The formation of a deposit on the membrane must be seen as the consequence of concentration polarization near the membrane. It is this transition that can be described as critical.

The described interactions were the main causes of the membrane fouling. It was thus necessary to develop fouling indicators to understand and anticipate the effect of the surface interactions in order to implement control measures to remedy this phenomenon by different ways. The resultant force of surface interactions causing fouling can be introduced into the model [1,10] either as a set of forces acting between two objects or as a pressure reflecting a collective objects behavior between which interactions exist. In the first case, it is possible to introduce the surface energy between an object and a surface in order to model the effect of interactions on the transport in the vicinity of a surface.

This type of modeling was developed by Schippers and Verdouw [10]; they demonstrated experimentally that it is

possible to introduce a parameter in the filtration cake model on one hand, and theoretically the existence of a critical flow in tangential filtration of colloids on the other hand [1]. Moreover, interaction mechanisms exist at different levels in the mixture constituting the material fouling the membrane, namely solvent molecules, ions and molecules assemblages (macromolecules/particles). Depending on a large number of surface interactions (interactions couples), various phenomena are involved [26].

The experimental conditions are the transmembrane pressure $\Delta P_m = 2 \times 10^5$ Pa, the maximum volume filtration in the tank $V = 20$ L, the temperature $T = 25^\circ\text{C}$, the conductivity of surface water $K = [29; 584]$ $\mu\text{S cm}^{-1}$, pH = [6.20; 7.71], the ionic composition, i.e., iron, calcium and magnesium from the concentration in entire filtered water [0.23; 3.07] mg/L; [1.16, 44.63] mg/L and [0.62, 16.14] mg/L, respectively.

2.3. New formulation description

2.3.1. Approach based on the phenomenology of the surface

The adsorption phenomenon plays an important role in the mechanism of fouling of ultrafiltration or microfiltration membranes, the tangential filtration membranes which, by their nature, are microporous. Indeed, for loaded membranes having attractions with the medium to be filtered, capillary forces can compensate and even surpassed the action of gravity. The importance of the cohesion forces by capillarity occurs also at the scale of a small macroscopic sample. In addition, surface phenomena occur at the interface between either two immiscible liquids, or a liquid and a solid. The liquid–solid interface behaves as a stretched membrane characterized by surface energy, which is responsible of macromolecules deformations [29].

As in the linear filtration models formulated by Darcy and the fouling indicator, it is possible, following the same approach to include a new parameter in the Darcy equation of filtration in order to quantify and qualify the multiple interactions and all forces involved in the fouling process [30–33].

All these resultant forces and the multiple interactions traduce the mass transfer by means of an equation including both physical and physicochemical parameters, such as the transmembrane pressure, the surface energy, the cumulative filtered volume, the cake resistance, the overall thickness and the membrane surface. This equation constitutes a first step and is formulated by analogy to the equations of Schippers and Verdouw [10] and of Pradanos et al. [20]. From this analogy, two equations can be drawn expressing the overall surface energy involved. The second expression is developed based on a rearrangement of the law of Bernouilli.

Eqs. (6), (7) and (9) allow to describe continuously the accumulation of the material in the polarization layer and the deposit compression [34].

The fouling in stationary, transitional and turbulent state when the cake became compressible during the tangential filtration is described. This modeling is performed by describing the accumulation in a direction perpendicular to the surface. In this case, the tangential flow is bounded by the thickness of the diffusional boundary layer. Inspired from the filtration model of Shirato et al. [11] and of Li et al. [18], a new formulation

by incorporating a subscript I (m^{-2}) in the tangent leading to the development of the membrane fouling membrane fouling index ($\text{MFI}_{0.45}$) is proposed. The reformulated model allows to have the same linearity than the original model.

In addition, Salinas-Rodriguez et al. [35] proposed a new equation for the determination of the MFI, which became MFI–UF and cross-flow sampler MFI (CFS–MFI).

They indicated the presence of a fouling phenomenon, based on the adsorption on the surface and inside the pores. Also, the effect of the morphology of the membrane surface on the fouling of organic membranes was envisaged by Boerlage et al. [36] and Koo et al. [37]. The analysis of the phenomena involved in the separation membrane for the case of ceramic membranes and PES allows to establish the mathematical equation of the overall energy generated by the surface phenomena during the separation.

$$\frac{1}{\gamma} = \frac{\alpha \cdot \text{MES} \cdot L}{\Delta P_m} \quad (6)$$

Substituting Eq. (6) in Schippers and Verdouw's equation of the filtration model, to the development of the $\text{MFI}_{0.45}$ the classic filtration model has been reformulated (Eq. (7)):

$$\frac{t}{V} = \frac{\mu \alpha \text{MES}}{2S^2 \Delta P_m} V + \frac{R_m \mu}{S \Delta P_m} \quad (7)$$

The new formulation of Schippers and Verdouw's model including surface energy in the structural for the prediction of this parameter is given by Eq. (8):

$$\frac{t}{V} = \frac{\mu}{\gamma \cdot LS^2} \cdot V + \frac{R_m \mu}{S \Delta P_m} \quad (8)$$

Substituting Eq. (8) in Eq. (6) leads to Eq. (9):

$$\gamma = \frac{\Delta P_m}{R_c \cdot S \cdot L} V \quad (9)$$

It represents the predictive surface energy model in the tangential cake filtration.

In the light of the work of Schippers and Verdouw [10] for the cake filtration using an indicator of fouling I (m^2) and the work of Elimelech et al. [38] by neglecting the osmotic pressure against the transmembrane pressure and the resistance corresponding to the pores blockage against the progressive resistance, the ratio of the cross-flow, the cake and the membrane resistance can be defined by Eqs. (10) and (11):

$$\frac{J_{po} - J_{pc}}{J_{pc}} = \frac{R_c}{R_m} \quad (10)$$

$$R_c = \alpha m_c = \alpha \text{MES} \frac{V}{S} \quad (11)$$

Furthermore, in the work of Jogdand and Chaudhuri [39], they proposed a model in which they considered the osmotic pressure included in the permeate pressure (P_p) (Eq. (12)):

$$P_p = P_{\text{atm}} + \Delta \pi \quad (12)$$

where $\Delta\pi$ is the difference in osmotic pressure of the solution at the membrane (π_{mem}) and in the permeate (π_{perm}): $\Delta\pi = \pi_{\text{mem}} - \pi_{\text{perm}}$ (kPa).

2.3.2. Approach based on the dynamic flow

The tangential filtration was performed based on the hypothesis of the dynamics of real fluids [40]. Various forces acting in the process resulting from the movement of the fluid to the surface of the membrane, leading therefore to a loss of singular and linear pressure [41]. In addition, the interactions responsible for the energy of Dupré in the turbulent regime, uniformity of speed allows to rearrange the Bernoulli equation for the transfer of the amount of movement by considering the tangential rate (U_t) as maximum throughout the process. Thus, the equation is as follows:

$$\frac{U_t^2}{2} + \frac{P_2 - P_1}{\rho} + g \cdot x = J_{12} = -\lambda \cdot \frac{U_t^2}{2} \left(\frac{L}{d_e} \right) \quad (13)$$

Several authors proposed a simplified equation of the transmembrane pressure expression, defined as the average of the inlet and the outlet pressure minus atmospheric pressure of the permeate compartment (Eq. (14)). From this approximation, the transmembrane pressure was considered homogeneous throughout the surface of the membrane. The characteristics of the membrane, namely the porosity and the real nature of the fluid to be filtered as in the case of fermented medium, suggests that the membrane is totally smooth and the mechanical force acting upon the thickness of the membrane is constant over time and is not bounded in any way to the cake formation.

$$\Delta P_m = \frac{P_1 + P_2}{2} - P_{\text{atm}} \quad (14)$$

In addition, Benkahla et al. [42], and Hamachi and Mietton-Peuchot [43] studied the influence of the transmembrane pressure on the porosity and the thickness of a deposit formed by a suspension of CaCO_3 in a microfiltration tangential mode. They observed that when the pressure increased, the porosity of the formed layer decreased and the increase in pressure lead to an increase in the thickness of the deposit up to a limit value. This value is due to the balance between the force applied by the transmembrane pressure and the shear force created by the recirculation speed.

In addition, in tangential ultrafiltration (UFT), Hamachi et al. [44] and Marselina et al. [45] found that for the same volume filtered, the thickness of the deposit increased with the concentration of the filtered suspension. Marselina et al. [45,46] in their study obtained the same results and concluded that the transmembrane pressure increased as a function of thickness.

Also, Hong and Elimelech [34] suggested another expression of the transmembrane pressure. They took into account the pressure related to the presence of particulate fouling the membrane and the pressure related to the polarization. This pressure is therefore the real transmembrane pressure of operation (Eq. (15)).

Therefore, this linearity between the transmembrane pressure and the thickness must be expressed in order to

describe the real phenomenological behavior of the system and its characteristics, namely expressing the transmembrane pressure as a function of the evolution of the overall thickness and the filtration length:

$$\Delta P_m = \left(\frac{P_2 - P_1}{x} \right) * L + P_p = \left(\frac{P_2 - P_1}{x} \right) * L + (P_{\text{atm}} + \Delta\pi) \quad (15)$$

This expression takes into account all the characteristic parameters, the operating pressure before and after the cake formation. Thus, by substituting in Eq. (13), Eq. (16) was obtained.

In Eq. (16), transmembrane pressure can be expressed in terms of the overall energy. The importance of Eq. (17) allowed to determine the variation of transmembrane pressure according to overall energy and filtered volume in fouling process and filtration process.

$$\frac{U_t^2}{2} + \left(\frac{\Delta P_m - (P_{\text{atm}} + \Delta\pi)}{\rho \cdot L} \right) * x + g \cdot x = -\lambda \cdot \frac{U_t^2}{2} \left(\frac{L}{d_e} \right) \quad (16)$$

$$\Delta P_m = \frac{\gamma \cdot R_c \cdot S \cdot L}{V} \quad (17)$$

2.3.3. Expression of the filtration kinetics equation

The combination between Eqs. (9), (13), (15), (16) and (17) and the substitution of the transmembrane pressure in the rearranged Bernoulli equation yields Eq. (18):

$$\gamma = -(B) * \left(\frac{V}{t} \right) + \frac{(P_{\text{atm}} + \Delta\pi) \cdot \theta_i}{2R_c \cdot S \cdot L} = \frac{\Delta P_m}{R_c \cdot S \cdot L} \quad (18)$$

Thus, by setting the cumulative volume from Eq. (18) described above, a rearrangement of Eq. (18) yields to Eq. (19). Considering that the kinetic is of order $n = 1$, the general expression of the cake is represented by the following equation:

$$\left(\frac{dV}{dt} \right)^n = -A_1 \left(\frac{d \left(\frac{V}{t} \right)}{dt} \right)^n + A_2 \quad (19)$$

2.4. Parametric study

This formulation describes the kinetics of the tangential filtration in a linear way namely the pore blockage model expressed by $1/V = f(1/t)$, the standard pores blockage model $t/V = f(t)$ and the filtration cake model taken as reference in this work $t/V = f(V)$.

According to Huang and Thomas [47], a linear relationship between $t/V = f(V)$ can be observed during the initial step of cake formation. After equilibrium, t/V is independent of V , and the relationship is not linear. The parameters allowing optimizing the process in order to obtain the convergence of the model are determined using Eq. (20) of Kozeny–Carman and the general Eq. (21) of Ergun [48]:

$$\alpha = \frac{180(1-\varepsilon)}{\rho d_p^2 \varepsilon^3} \quad (20)$$

$$\frac{\Delta P}{L} = \left(\frac{150(1-\varepsilon)^2 \mu}{\varepsilon^3 d_p^2} \right) U_t + \left(\frac{1,75(1-\varepsilon)\rho}{\varepsilon^3 d_p} \right) U_t^2 \quad (21)$$

2.4.1. The tangent (A_t)

The descriptive model curve ($V = f(V/t)$), which reflects the linearity obtained in this modeling process, allows to determine the relevant parameters to describe the process of the tangential filtration of membrane fouling and the overall physical that governs the mechanisms involved in the separation process.

A rearrangement of Eq. (19) allows to achieve Eq. (22) and finally Eq. (23). Eq. (22) was obtained by translation of various parameters derived from Eq. (18) in the general Eq. (21) of Ergun [48] and by substituting other parameters by applying the Kozeny–Carman equation (Eq. (20)) on the hydraulic resistance α (m/kg) of the fouling cake. Thus, after several mathematical transformations, after setting the characteristic of the tangential filtration process and the fouling, Eq. (24) is finally obtained.

$$V = \left(- \frac{45\gamma \text{MES} L (x\lambda + d_e)}{150\mu(1-\varepsilon)d_e \Delta P_m + 1,75d_e \Delta P_m \rho d_p U_t} \right) * \left(\frac{V}{t} \right) + \frac{(P_{\text{atm}} + \Delta\pi) v_i}{2\Delta P_m} \quad (22)$$

$$\Psi = \frac{45(x\lambda + d_e)}{150\beta d_e + 1,75R_e d_p} \quad (23)$$

In Eq. (23), Ψ is a dimensionless grandeur characteristic of the membrane, the flow regime and the type of medium to be filtered (colloidal particles, spherical, etc.). The parameter Ψ characterizes the fouling power of the filtered fluid according to the training and the settlement of the cake. The value of Ψ is between 0 and 1, and its analytical expression is given by Eq. (24):

$$V = \left(- \left(\frac{\gamma \text{LMES}}{\mu \Delta P_m} \right) * \Psi \right) * \left(\frac{V}{t} \right) + \frac{(P_{\text{atm}} + \Delta\pi) v_i}{2\Delta P_m} \quad (24)$$

This model is a deterministic model because all the considered assumptions are derived from the analysis of the phenomenology of the filtration system combined with the nature of the medium (fluid and its characteristics). In addition, the resistances are in series that allows taking into account their overall effect during the process of filtration and fouling [34,35].

2.4.2. Overall thickness estimation

A study on the frontal filtration of domestic wastewater showed linearity between the thickness of the formed cake and the filtered volume [49]. The same observation was made by Tien and Ramarao [50]. Therefore, the thickness

of the membrane combined with the deposit fouling can be expressed according to an integral of the form:

$$L = e_m + \int_0^t e_c(t) \cdot dt \quad (25)$$

By combining Eqs. (9), (18), (20), (21), (22) and (24), the linear expression between the overall thickness of the filtered volume is given by Eq. (26):

$$e_c = \left(\left(\frac{\Delta P_m \text{MES} x d_e}{4R_e S \gamma \mu} \right) * \Psi \right) \left(\frac{V}{t} \right) - \frac{(P_{\text{atm}} + \Delta\pi) + e_m R_e S V P}{R_e S V P} \quad (26)$$

2.5. Model validation

The validation of the model constitutes the critical step in the modeling process. Thus, the procedure consists in plotting V vs. V/t from the experimental data using OriginPro Ver. 8 software. The comparison between the predicted and the experimental values, along with the determination of the absolute relative errors and R^2 /adjusted R^2 , allowed to demonstrate the effectiveness of the proposed model and to determine the level of convergence toward cake filtration model. The application of the model was carried out on experimental data obtained from the work of Professor Christian Bouchard of Laval University, Canada, Civil Engineering Department. These data were obtained during a comparative study of fouling in nanofiltration and in UFT.

In addition, based on the correlation coefficient models obtained by Pradanos et al. [20] and Tien and Ramarao [50], the reproducibility and the performance of the new model were compared with the existing models. Finally, the validation model focused on the analysis of the distribution function of the variance (ANOVA), the evaluation of relative errors and the error probability on the variance.

3. Results and discussion

The formulated model was applied depending on the assumptions and the considered hydrodynamic regime. The new model proposed was applied on 23 cases of tangential filtration, 10 cases of ultrafiltration and 13 cases of nanofiltration.

3.1. Validation of the model on tangential ultrafiltration

The application of the new proposed model to surface water ultrafiltration revealed the three typical phases of the filtration process (Fig. 1). According to the trajectory of the characteristic curve of the model (Eq. (24)), the three phases were linear and described the different mechanisms involved in this new model (Eq. (24)).

Therefore, the fouling process did not occur in two phases or two flows as usually shown in the literature. As can be seen from Fig. 2(b), the filtration process was not carried out in three laws; each gave an account for an intrinsic phenomenon that occurred. Also, the model followed perfectly the experimental data in all cases that allows to conclude that the calculated values were in agreement with the experimental ones.

Table 1 shows that the absolute relative errors obtained from the proposed model are significantly higher compared with those found by Schippers and Verdouw [10] reflecting a more accurate description of the UFT with this new model. This was illustrated at the examination of Fig. 2(a), confirming the relevance of the new model. The surface phenomena involved in the tangential filtration process with the membrane characteristics in combination with the transport phenomena allowed therefore the construction of an effective and efficient model.

Indeed, the new model showed that the pore blockage was progressive and not fast as described by Hermia [9]. Thus, on a set test of 11 cycles, each in UFT, according to the obtained results, it is possible to site a different phase of blockage pores around of an average of 40% of filtration cycles, because similar behavior was observed in experimental data treated from all UFT assays in the same operating condition. According to several studies of Tien et al. [51] and of Daniel et al. [52], the results given in Tables 1 and 2 are statistically significant for the new model fitting in a confidence interval of 95%.

Moreover, this blockage occurred in two phases, preceding the establishment of the fouling cake. This can be

explained by the fact that the surface energy is proportional to the filtered volume and the complete obstruction of the pores was observed only when this energy reached its maximum, by the increase of the capillary force and the multiple interactions forces exerted inside the pores and gradually on the membrane surface [25,50,52].

Table 1 summarizes the results of the variance analysis of the 10 tests of UFT.

The new established model described a logistic growth in the process of membrane fouling with an increase in three phases, which confirmed its performance and accuracy. The formation of fouling was preceded in all filtration tests by a step delimiting the complete blockage of the pores determining the change of hydrodynamics.

In addition, the estimated error on the variance function was of the order of 10^{-11} – 10^{-15} , showing the conformation of the calculated values with the experimental data. The absolute relative error calculated on the ultrafiltration data was found to be in the range of 1.21%–9.20% (Table 1) with a correlation coefficient of 99.97% and 99.79%, respectively.

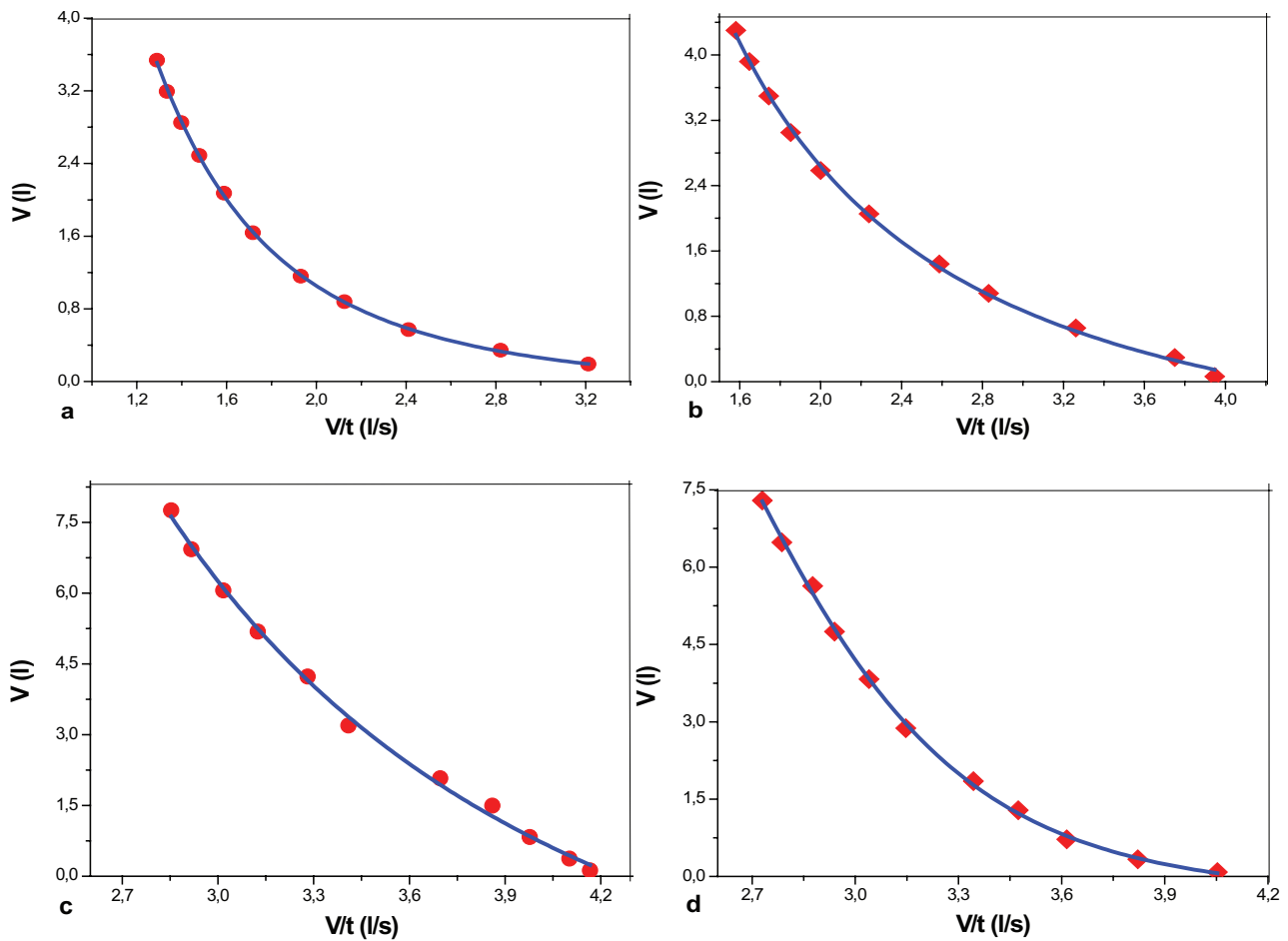


Fig. 1. New model behavior (V vs. V/t) according to tangential ultrafiltration (UFT) assays of surface water on polyethersulfone membrane: (a) first assay (● experimental values and — model fitting); (b) third assay (■ experimental values and — model fitting); (c) ninth assay (● experimental values and — model fitting) and (d) tenth assay (■ experimental values and — model fitting). Note: $T = 25^\circ\text{C}$; $R_m = 8.140 \times 1,013 \text{ m}^{-1}$; $\Delta P_m = 2 \times 105 \text{ Pa}$; $U_t = 0.111 \text{ m s}^{-1}$; $J_0 = 3.5 \times 10^{-5} \text{ m s}^{-1}$; $K = 1.92 \times 10^{-10} \text{ m/s Pa}$; and $Q = 0.5 \text{ L/min}$.

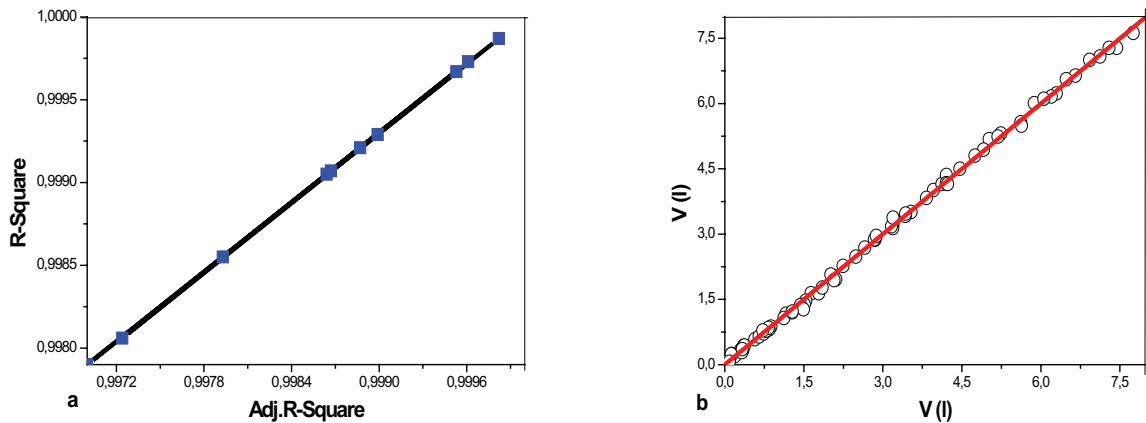


Fig. 2. (a) the R^2 against the adjusted R^2 and (b) model calculated values against experimental values of the cumulative volume ($y = 0.99919 \times x + 0.00297$) in UFT of surface water on polyethersulfone membrane.

Note: $T = 25^\circ\text{C}$; $R_m = 8.140 \times 1,013 \text{ m}^{-1}$; $\Delta P_m = 2 \times 105 \text{ Pa}$; $U_f = 0.111 \text{ m s}^{-1}$; $J_0 = 3.5 \times 10^{-5} \text{ m s}^{-1}$; $K = 1.92 \times 10^{-10} \text{ m/s Pa}$; and $Q = 0.5 \text{ L/min}$.

Table 1

Analysis of variance (ANOVA) of the data applied on the new model in ultrafiltration and comparison with Schippers and Verdouw [10] and Pradanos et al. [20] models

ANOVA					Statistical analysis data					
No. of assay	Sum of square	Mean square	F value	Prob. > F	R^2 adjusted		R^2		Relative error	
					Model	Schippers	Model	Schippers	Model	Schippers
1	46.6120	11.6530	22,178.2551	2.77556E-14	0.9996	0.9715	0.9997	0.9744	0.0121	0.0832
2	89.2326	22.3081	7,431.6276	1.27531E-12	0.9990	0.9867	0.9993	0.9880	0.0395	0.0613
3	70.0378	17.5094	5,925.5063	2.81664E-12	0.9987	0.9962	0.9991	0.9966	0.0797	0.0605
4	78.7523	19.6881	5,816.7266	3.00526E-12	0.9986	0.9982	0.9990	0.9984	0.0572	0.0542
5	126.4705	31.6176	15,434.3031	9.88098E-14	0.9995	0.9839	0.9997	0.9855	0.0891	0.0484
6	193.9435	48.4859	2,582.2757	5.14525E-11	0.9972	0.9976	0.9981	0.9978	0.0858	0.0246
7	137.3014	34.3253	3,464.7378	1.84059E-11	0.9979	0.9769	0.9985	0.9792	0.0745	0.0505
8	215.8073	53.9518	17,231.9794	6.72795E-14	0.9996	0.9707	0.9997	0.9736	0.0536	0.0298
9	206.9808	51.7452	2,324.8711	7.42764E-11	0.9970	0.9942	0.9979	0.9947	0.0920	0.0229
10	178.0852	44.5213	5,974.7653	2.73626E-12	0.9989	0.9513	0.9992	0.9562	0.0596	0.0371

3.2. Validation of the model for tangential nanofiltration

The application of the new model to the nanofiltration of surface water revealed that the fouling process and/or the filtration involved also three characteristic phases (Fig. 3), as observed in ultrafiltration.

This corroborates the general character of this model. Thus, the linear character observed in nanofiltration was due to the significant difference in transmembrane pressure [43,44] because the porosity of the membrane was lower in this case. In fact, the nanofiltration was carried out after a compaction or pre-filtration in UFT mode in order to shift from the nanofiltration to the UFT with the same membrane.

Thus, the behavior of the model against the experimental values was the result of the fouling cake formation from the ultrafiltration beforehand performed. The experiences were led by Pradanos et al. [20] having supplied treated data in this study and bringing back a loss of 24% permeability in ultrafiltration and 21% in nanofiltration. It explains that initial pore blockage phase was unobserved after pre-filtration in UFT mode and a complete blockage as shown in Fig. 3 during nanofiltration.

As for the case of the ultrafiltration, the new model applied on the nanofiltration described a logistic growth of the membrane fouling process with the increase in the fouling cake. Thus, according to the study of Schippers and Verdouw [10], the formation of the cake resulted in the appearance of a characteristic linearity of the incompressible cake. This linearity was lost when the cake became compressible.

This result is in agreement with the description made by Tien and Ramarao [50] confirming the performance and the accuracy of the new model, able to describe change in the phenomenological behavior of the system. Furthermore, the ANOVA showed a great improvement of the model in the context of its generalization following the growth of the energy of Dupré and the thickness of the fouling cake. The error probability on the variance function was of the order of 10^{-9} – 10^{-14} . The absolute relative error calculated on the data from the nanofiltration was in the range from 2.7% to 9.93% with a correlation coefficient of 99.82% and 99.97%, respectively (Table 2).

The models of Schippers and Verdouw [10] and Pradanos et al. [20] and Eq. (7) due to their identical architecture

Table 2
ANOVA of the data applied on the new model in nanofiltration

ANOVA					Statistical analysis data					
No. of assay	Sum of squares	Mean square	F value	Prob. > F	R ² adjusted		R ²		Relative error	
					Model	Schippers	Model	Schippers	Model	Schippers
1	105.5384	26.3846	991.0269	1.46107E-9	0.9933	0.9696	0.9953	0.9726	0.0853	0.0201
2	40.8475	10.2119	2,607.2050	4.97528E-11	0.9975	0.6754	0.9982	0.7078	0.0993	0.2373
3	110.0937	27.5234	12,251.3742	2.21823E-13	0.9994	0.9963	0.9996	0.9966	0.0414	0.0426
4	125.6754	31.4188	5,297.6774	4.16767E-12	0.9986	0.9969	0.9990	0.9973	0.0465	0.0374
5	85.6498	21.4125	7,468.2399	1.25355E-12	0.9990	0.9936	0.9993	0.9942	0.0549	0.0577
6	91.3200	22.8300	2,164.4068	9.5375E-11	0.9965	0.9946	0.9975	0.9952	0.0894	0.0516
7	96.1126	24.0282	6,521.1487	2.01461E-12	0.9988	0.9970	0.9992	0.9973	0.0758	0.0511
8	140.6494	35.1623	14,997.7897	1.09246E-13	0.9995	0.9991	0.9996	0.9992	0.0317	0.0274
9	225.3474	56.3369	1,939.8925	1.39858E-10	0.9964	0.9921	0.9975	0.9929	0.0852	0.0190
10	155.0235	38.7559	2,700.6745	4.39875E-11	0.9973	0.9968	0.9981	0.9972	0.0632	0.0236
11	251.3168	62.8292	1,337.1438	5.13302E-10	0.9951	0.9838	0.9966	0.9854	0.0776	0.0159
12	187.2987	46.8247	2,059.4729	1.1347E-10	0.9968	0.9397	0.9977	0.9457	0.0595	0.0277
13	171.1679	42.7920	19,230.2343	4.57412E-14	0.9996	0.9969	0.9997	0.9972	0.0297	0.0270

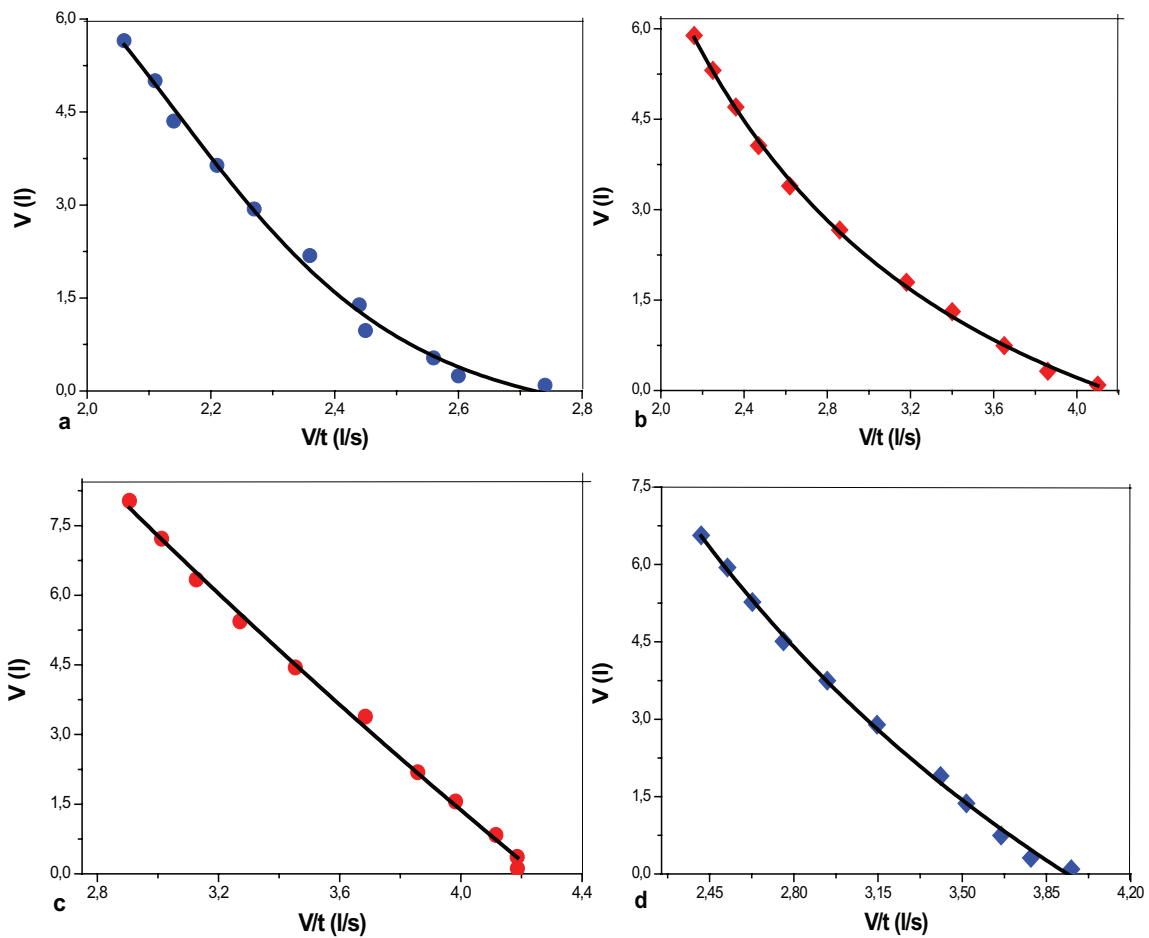


Fig. 3. New model behavior (V vs. V/t) according to tangential nanofiltration of surface water on polyethersulfone membrane: (a) first assay (● experimental values and — model fitting); (b) fourth assay (■ experimental values and — model fitting); (c) ninth assay (● experimental values and — model fitting); and (d) tenth assay (■ experimental values and — model fitting).
Note: $T = 25^{\circ}\text{C}$; $R_m = 8.140 \times 1,013 \text{ m}^{-1}$; $\Delta P_m = 2 \times 105 \text{ Pa}$; $U_t = 0.111 \text{ m s}^{-1}$; $J_0 = 3.5 \times 10^{-5} \text{ m s}^{-1}$; $K = 1.92 \times 10^{-10} \text{ m/s Pa}$; and $Q = 0.5 \text{ L/min}$.

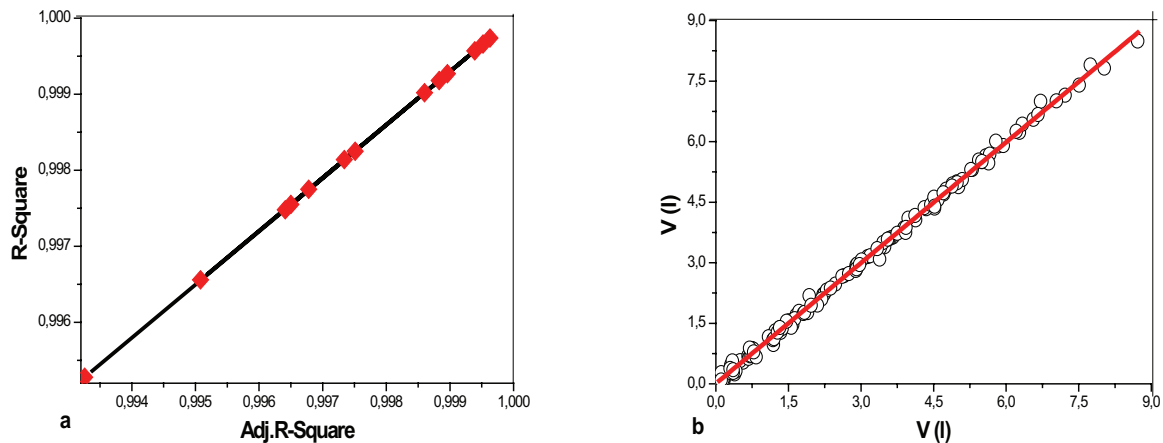


Fig. 4. (a) The R^2 against the adjusted R^2 and (b) model calculated values against experimental values of the cumulative volume ($y = 0.99665 \times x + 0.0068$) in tangential nanofiltration of surface water on polyethersulfone membrane.

Note: $T = 25^\circ\text{C}$; $R_m = 8.140 \times 1,013 \text{ m}^{-1}$; $\Delta P_m = 2 \times 105 \text{ Pa}$; $U_t = 0.111 \text{ ms}^{-1}$; $J_0 = 3.5 \times 10^{-5} \text{ m s}^{-1}$; $K = 1.92 \times 10^{-10} \text{ m/s Pa}$; and $Q = 0.5 \text{ L/min}$.

showed an absolute relative error between 23.73% and 2.01% with a correlation coefficient of 70.78% and of 99.42%, respectively (Table 2).

The obtained results from the variance and the statistical analysis on the data of nanofiltration are depicted in Table 2.

Fig. 4(b) highlighted clearly the correlation between the predicted values from the proposed model and the applied experimental values. Thus, it corroborates the accuracy of the new model to describe the phenomenon of the filtration and of the fouling process in the tangential mode. Therefore, this model perfectly described both applications and the influence of the global surface energy involved in this process and confirmed the preponderance of the surface phenomena on the dynamics adsorption caused during the fouling process with regard to the studies of Li et al. [2] and Maloberti [26].

3.3. Evaluation of the filtration pressure

The ratio of the pressure, which resulted from the filtration law established in this work, allowed determining the mechanical conditions of the filtration process in the two studied cases. Furthermore, this ratio can be determined from the intercept and the elementary filtered volume at each filtering cycle in the case of the developed model.

Eq. (24) showed that the transmembrane pressure was not constant and varied with the number of cycles performed, while the pressure of the permeate compartment remained atmospheric (in the normal conditions).

According to the obtained results, the pressure was not constant throughout the process and monitored the fouling evolution according to both its nature and type. Assuming that the pressure of the permeate compartment was constant; this showed the increase of the transmembrane pressure until reaching a maximum, which characterized the beginning of the formation of the fouling cake.

Fig. 5 shows the evolution of the pressure ratio based on the cumulative filtered volume, which appeared in close agreement with the established tangential filtration law in this work. In fact, the behavior of the transmembrane pressure was identical to that described by Hong and Elimelech

during tangential filtration [34]. In addition, the transmembrane pressure was proportional to the overall surface energy and the thickness of the fouling cake, confirming that this pressure increased during the formation of the incompressible cake. However, the fall of pressure observed in both cases was the consequence of the formation of a compressible cake [37]. Before this formation, pores blockage provoked a rise of the pressure due to the incompressibility of the cake formed on the surface of the membrane.

From Fig. 5, the cake compressibility has an intrinsic relation of osmotic compressibility due to the increase of the osmotic pressure. It is well known that the increase in the shear rate on the membrane surface reduces the polarization of the solute concentration and consequently the osmotic pressure [39]. The osmotic pressure as a function of concentration and diffusional coefficient of the solute described the osmotic compressibility between the permeate and the retentate.

Furthermore, the ratio of the pressure vs. the elementary volume was linear. A rearrangement of Eq. (24) allowed to obtain Eq. (27) that described the pressure ratio against the elementary volume:

$$\frac{\Delta P_m}{(P_{\text{atm}} + \Delta\pi)} = \frac{1}{2} \left(\frac{v_i}{V} \right) \quad (27)$$

Fig. 6 demonstrates that the transmembrane pressure as well as the permeate compartment pressure varied significantly according to the filtered volume. This description confirms the assumption considered for the formulation of Eq. (15), dealing with the evolution of the report $(\Delta P_m / P_{\text{atm}} + \Delta\pi)$ characterizing the membranes fouling power according to the filtration assay number. The fouling following Fig. 6 results (a), (b), (c) and (d) reached an irreversible level when the report of pressure establishes itself with the volume initially filtered in both cases. In the light of the results found, the transmembrane pressure was more important in nanofiltration than in UFT. The three cross-flow phases described in the hypothesis and in the application on the ultrafiltration and the tangential nanofiltration (NFT) were demonstrated by evaluating the pressure ratio vs. the inverse cumulative

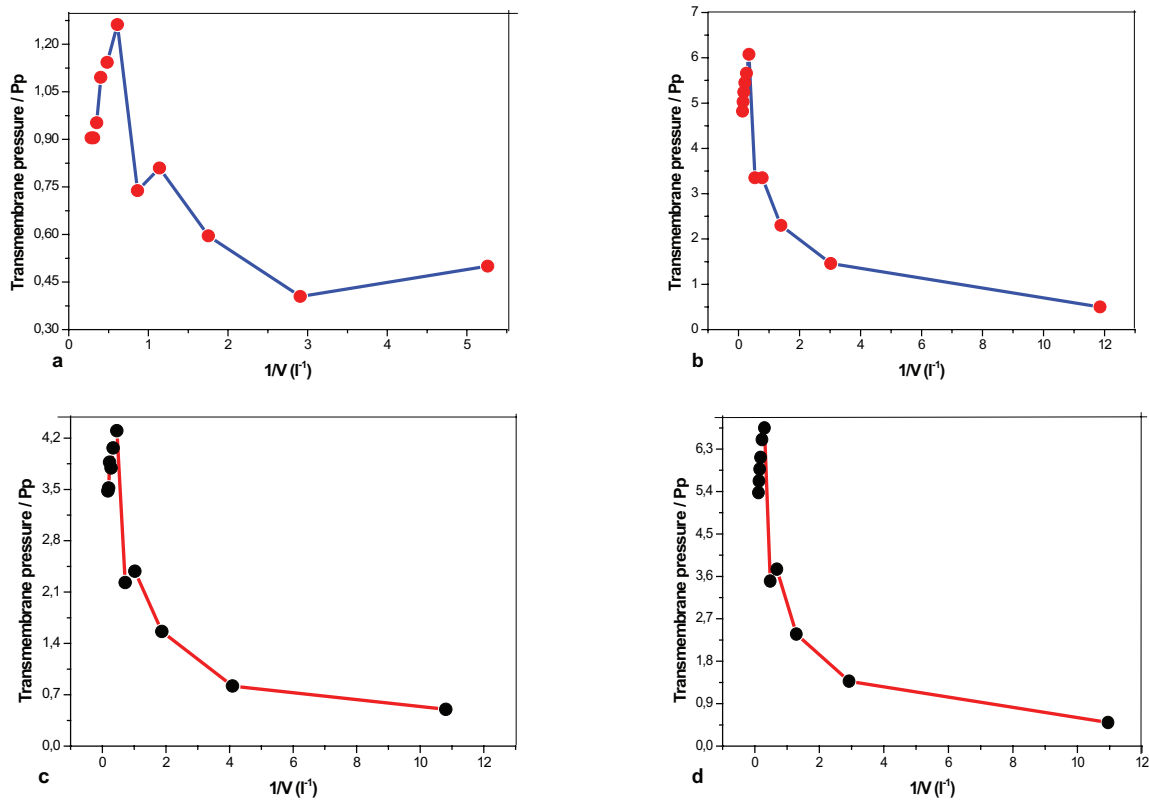


Fig. 5. (a) and (b) Transmembrane pressure jump against the inverse of cumulative volume in UFT, and (c) and (d) tangential nanofiltration on polyethersulfone membrane with the constant permeate pressure compartment.

Note: $T = 25^{\circ}\text{C}$; $R_m = 8.140 \times 1,013 \text{ m}^{-1}$; $\Delta P_m = 2 \times 10^5 \text{ Pa}$; $U_f = 0.111 \text{ m s}^{-1}$; $J_0 = 3.5 \times 10^{-5} \text{ m s}^{-1}$; $K = 1.92 \times 10^{-10} \text{ m/s Pa}$; and $Q = 0.5 \text{ L/min}$.

volume. Indeed, Fig. 6 shows an increase of the pressure in three distinct phases that confirmed all the assumptions set out in this work.

3.4. Prediction of the surface energy (γ) and the fouling power (Ψ)

The fouling characterized by parameters γ and Ψ were estimated according to the final value of thickness for all filtration assays. In the experimental study conducted by Pradanos et al. [20], dealing with ultrafiltration and nanofiltration, the values of the thickness are not given.

In this case, according to Lodge et al. [53], the maximal thickness value obtained, and $200 \mu\text{m}$ was used.

From the study of Li et al. [2], the thickness value observed confirmed the first hypothesis and described well the three phases of cross-flow during the filtration process. The maximal thickness observed was of 362 nm with membrane initial thickness of 118 nm .

The model proposed a prediction of fouling parameters γ , which represents the anti-fouling characterizing the reverse energy required to remove the membrane fouling and Ψ representing the fouling power according to the characteristics of the membrane system, the hydrodynamic of the system and the fluid filtration.

Fig. 7 represents the predictive values of surface energy following cumulative volume assay by assay of ultrafiltration (Fig. 7(a)) and nanofiltration (Fig. 7(b)). The results obtained demonstrate that surface energy was most important in the

fouling process in nanofiltration than in ultrafiltration ($\gamma = 58.80 \text{ mN m}^{-1}$, $R^2 = 0.995$ for UFT and $\gamma = 1,268.69 \text{ mN m}^{-1}$, $R^2 = 0.962$ for NFT). This trend was confirmed by the results of the fouling power (Fig. 8).

From Fig. 8, it was noticed that the membrane fouling was fast, and the membranes need to be cleaned after four filtrations assays in ultrafiltration ($R^2 = 0.951$). In nanofiltration ($R^2 = 0.999$), membrane did not show significant fouling before 10 filtrations assays.

To characterize the fouling process in the tangential filtration through combination of the surface energy and the power of fouling, the results indicate that less surface energy was sufficient to cause fouling in ultrafiltration than in nanofiltration, which required a high surface energy. It was due to the membrane surface morphology, the formation of incompressible cake following the compressible cake during filtration process and the effect of cut threshold of the membrane.

Logistics growth observed surface energy characterizes the fouling phenomenon in three phases. The first phase of the intermediate blocks defined pores or sanitation actions promoting the adsorption phenomena inside the pores under the influence of the energy of fouling, the second phase of incompressible cake training, which stabilized the bulk on the surface of the membrane, and the third phase of compressible cake formation or colonization action. The recirculation of the shear fluid caused a decrease in the permeation by a gradual loss of permeability with time.

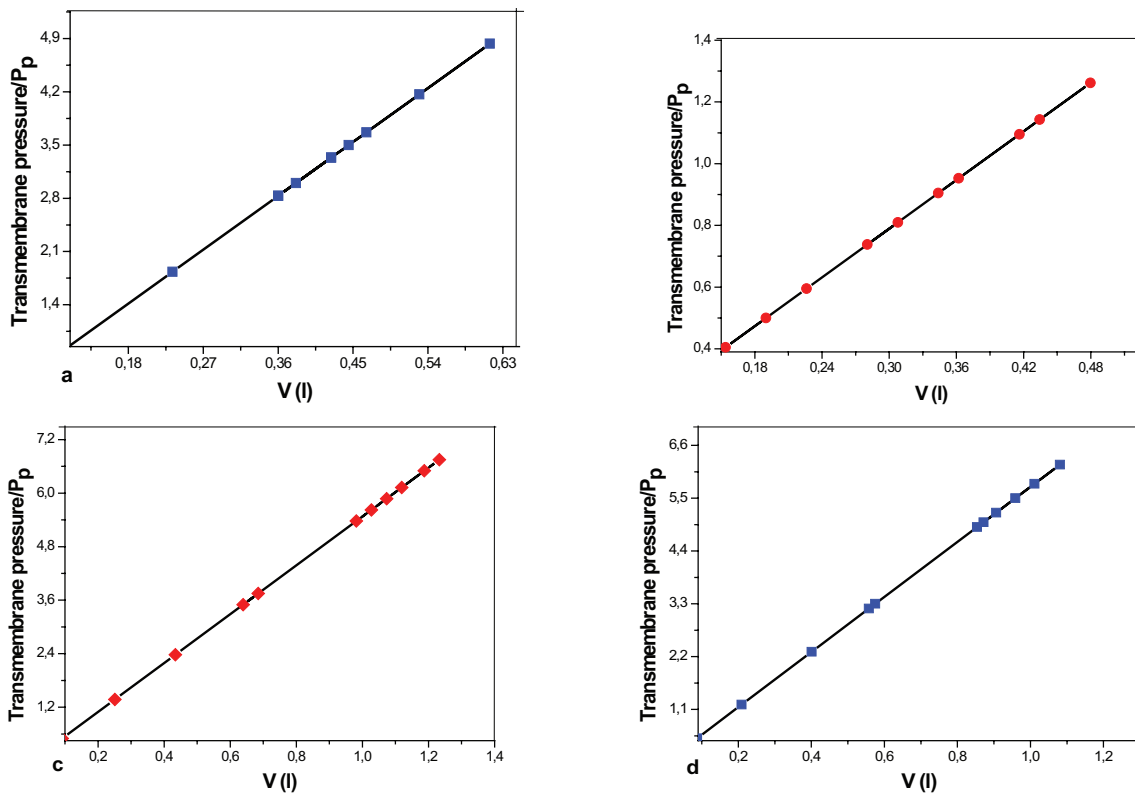


Fig. 6. (a) and (b) Transmembrane pressure ratio evolution on the permeate pressure compartment against the elementary volume in UFT and (c) and (d) tangential nanofiltration on polyethersulfone membrane.

Note: $T = 25^\circ\text{C}$; $R_m = 8.140 \times 1,013 \text{ m}^{-1}$; $\Delta P_m = 2 \times 10^5 \text{ Pa}$; $U_t = 0.111 \text{ m s}^{-1}$; $J_0 = 3.5 \times 10^{-5} \text{ m s}^{-1}$; $K = 1.92 \times 10^{-10} \text{ m/s Pa}$; and $Q = 0.5 \text{ L/min}$.

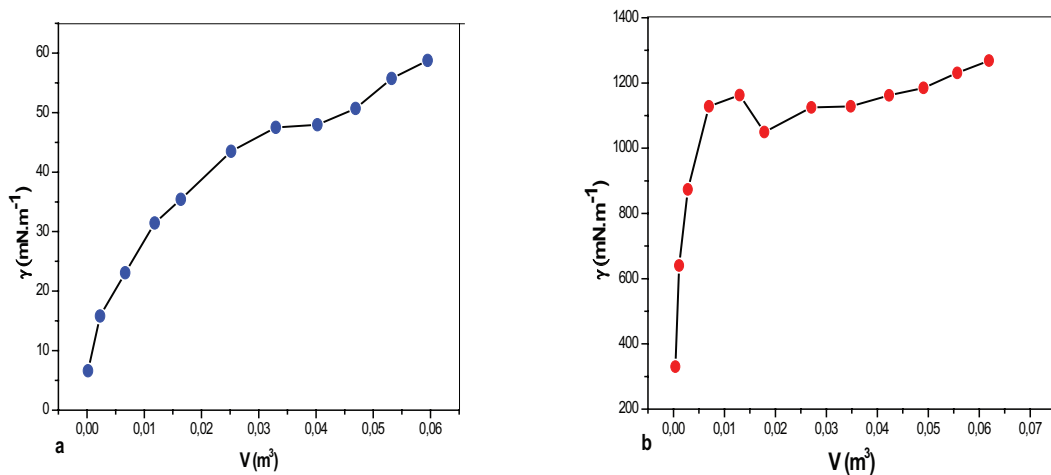


Fig. 7. (a) Surface energy for UFT and (b) surface energy for NFT according to cumulative volume assay by assay.

Note: $T = 25^\circ\text{C}$; $R_m = 8.140 \times 1,013 \text{ m}^{-1}$; $\Delta P_m = 2 \times 10^5 \text{ Pa}$; $U_t = 0.111 \text{ m s}^{-1}$; $J_0 = 3.5 \times 10^{-5} \text{ m s}^{-1}$; $K = 1.92 \times 10^{-10} \text{ m/s Pa}$; $Q = 0.5 \text{ L/min}$, $R_c = [2.09 \times 10^8; 7.33 \times 10^9]$ for UFT and $R_c = [8.29 \times 10^8; 3.53 \times 1,010]$ for NFT, and $L_{\max} = 200.244 \times 10^{-6} \text{ m}$ for all assays.

Beside this aspect, mass growth also resulted from the membrane cut threshold effect 300 kDa NFT and 10 kDa UFT. This cut threshold difference explained partially the fouling nature according to the membrane, because irreversible fouling in case of tangential filtration was profoundly dependent on the threshold. Indeed, He et al. [54] noticed using the atomic force microscope photography that more the cut threshold is important, more the roughness of the membrane

is important, and this rough morphology allowed collision of particles responsible of the fouling; this result was confirmed by Elimelech et al. [38].

According to the results of Fig. 5, the compressibility of the cake has an intrinsic relation of osmotic compressibility due to the increase in the osmotic pressure. Also the effect of the increase of the shear rate on the surface of the membrane reduces the polarization of the solute concentration and

therefore the osmotic pressure [39]. In addition, the osmotic pressure as a function of the concentration and the diffusion coefficient of the solute describes the osmotic compressibility between the permeate and the retentate. Recently, Chen et al. [55] described the effect of resistance induced by osmotic pressure. This mechanism has been reported by Hong et al. [56].

The osmotic pressure induced was included in the effect of the overall surface energy. Fig. 9, and Eqs. (28) and (29) demonstrate the proportionality of the overall surface energy and the osmotic pressure. The most important effect of osmotic pressure was observed when the flux declined due to the opposition of the specific filtration resistance due to the osmotic compressibility. This mechanism was governed by the overall surface energy. The osmotic pressure-induced resistance was proposed to be generated from the chemical potential, difference between the permeate and the fouling layer carrying abundant negatively charged functional groups [57]. The negatively charged functional groups in the fluid filtered associated the sulfone functional groups of PES-membrane (zeta potential) to provoke the membrane fouling

mechanism. This association of functional groups was the most important overall surface energy as described in Fig. 7, according to the multiples interactions particles–particles and particles–wall during the filtration process.

$$\Delta\pi = \left(\frac{2\Delta P_m}{v_i} \right) * (V) - P_{atm} \quad (28)$$

$$\gamma = \frac{\Delta\pi + P_{atm}}{2R_c \cdot S \cdot L} * (v_i) \quad (29)$$

Also, the results of Fig. 6 demonstrate that the osmotic pressure had no significant effect on the membrane cross-flow decline.

However, the overall surface energy decreased slowly with the increase of the retained solute concentration (Figs. 7(a) and (b)). Subsequently, the flow moved to the overall surface energy dominant stage where the flow of decline appeared again.

The linearity of the curves (a), (b), (c) and (d) in Fig. 6 linked to the elementary permeate volume confirmed this

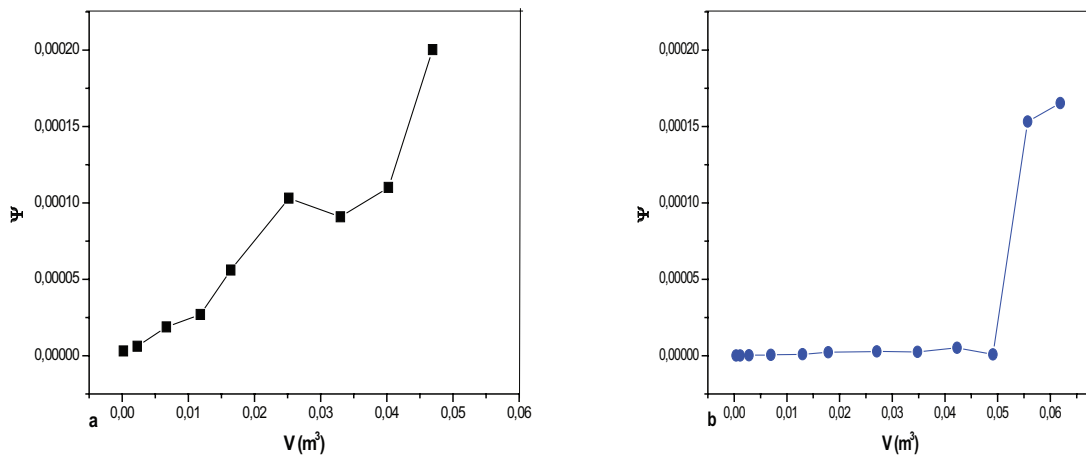


Fig. 8. Fouling power Ψ for UFT (a) and NFT (b) for all assays (assay by assay). Note: $T = 25^\circ\text{C}$; $R_m = 8.140 \times 1,013 \text{ m}^{-1}$; $\Delta P_m = 2 \times 105 \text{ Pa}$; $U_i = 0.111 \text{ m s}^{-1}$; $J_0 = 3.5 \times 10^{-5} \text{ m s}^{-1}$; $K = 1.92 \times 10^{-10} \text{ m/s Pa}$; $Q = 0.5 \text{ L/min}$, $R_c = [2.09 \times 108; 7.33 \times 109]$ for UFT and $R_c = [8.29 \times 108; 3.53 \times 1,010]$ for NFT, and $L_{max} = 200.244 \times 10^{-6} \text{ m}$ for all assays.

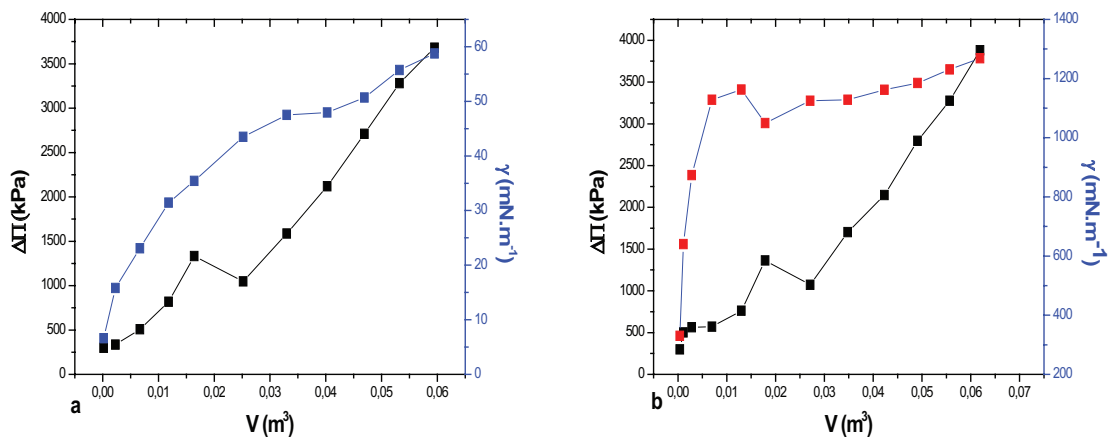


Fig. 9. Osmotic pressure $\Delta\Pi$ and overall surface energy γ for UFT ((a) with $R^2 = 0.9542$) and NFT ((b) with $R^2 = 0.9453$) for all assays (assay by assay). Note: $T = 25^\circ\text{C}$; $R_m = 8.140 \times 1,013 \text{ m}^{-1}$; $\Delta P_m = 2 \times 105 \text{ Pa}$; $U_i = 0.111 \text{ m s}^{-1}$; $J_0 = 3.5 \times 10^{-5} \text{ m s}^{-1}$; $K = 1.92 \times 10^{-10} \text{ m/s Pa}$; $Q = 0.5 \text{ L/min}$, $R_c = [2.09 \times 108; 7.33 \times 109]$ for UFT and $R_c = [8.29 \times 108; 3.53 \times 1,010]$ for NFT, and $L_{max} = 200.244 \times 10^{-6} \text{ m}$ for all assays.

behavior. Recently, in the beginning of the concentration process in the ultrafiltration of sugar [58], fouling formation by adsorption in/on the membrane of pigments and osmotic pressure increase were responsible for the rapid flux decline. The results are given in Fig. 5 according to the cumulative permeate volume; they confirmed this physical mechanism of fouling process. The permeate flux decreased due to the accumulation of small molecules in the concentrate by multiple particle surface interactions governed by the overall surface energy.

4. Conclusions

The proposed model allowed to demonstrate the impact of the overall surface energy in the fouling process of membranes. Surface phenomena considered in this study based on the surface energy were implemented in the process of membrane fouling according the multiple interactions: the characteristics of the adsorption process, the transport mechanism envisaged and the dynamical behavior of the membrane system filtration. From this, a new tangential filtration model was described.

The obtained results showed that the overall surface energy applied is the most important parameter for describing the fouling process of zeta potential membrane, more significant than the mechanical and gravitational forces considered in the classical formulation of fouling process and membrane filtration process modeling.

Otherwise, the result of the fouling power observed demonstrates that this parameter gave information about the evolution of the fouling power during filtration and the characteristics of fouling process based on the membrane characteristics and the fluid filtration. It was used to assess the level of change of the medium properties and the membrane during the filtration process.

The results of the osmotic pressure-induced fouling demonstrated that this mechanism is not important compared with the overall surface energy effect in the mechanism of the fouling process.

The various established equations appeared in adequacy with the physical reality of the filtration process and the membrane fouling. Furthermore, this study revealed that the transmembrane pressure in the case of tangential filtration on zeta potential membranes cannot be constant throughout the filtration process. Thus, the ANOVA provided consistent results on the error probability of data distribution function against the settings of monitoring in both cases: ultrafiltration and nanofiltration.

Symbols

\bar{C}_i	—	Average concentration of i in membrane, kg m^{-3}
C_i^f	—	Average concentration in membrane, kg m^{-3}
D_i	—	Diffusion coefficient of constitute i in membrane, $\text{m}^2 \text{s}^{-1}$
\bar{D}_i	—	Diffusion coefficient of element i in membrane, $\text{m}^2 \text{s}^{-1}$
d_e	—	Flow diameter, m
d_p	—	Pore diameter, m
F_i	—	Phenomenological associate force of Onsager theory, N

F_j	—	Phenomenological non-associate force of Onsager theory, N
g	—	Gravitational force, N Kg^{-1}
I	—	A Schippers modified fouling index, m^{-2}
J_i	—	Volume rate of flow solvent, $\text{m}^3 \text{s}^{-1} \text{m}^{-2}$
J_{p0}	—	Initial flow, m s^{-1}
J_{pc}	—	Permeate flow, m s^{-1}
K	—	Membrane permeability, $\text{m Pa}^{-1} \text{s}^{-1}$
L	—	Global thickness, m
L_{ij}	—	Phenomenological coefficient of Onsager theory
MES	—	Suspension matter, Kg m^{-3}
N	—	Pore number of surface membrane unit, m^{-2}
P	—	Applied pressure, Pa
P_1	—	Input pressure, Pa
P_2	—	Output pressure, Pa
P_p	—	Permeate compartment pressure, Pa
Q	—	Fluid flow supply, L/min
R	—	Constant of parfait gas, $\text{J mol}^{-1} \text{K}^{-1}$
R_m	—	Membrane resistance, m^{-1}
R_c	—	Cake resistance, m^{-1}
R_{ctotale}	—	Total cake resistance, m^{-1}
S	—	Membrane surface, m^2
T	—	Temperature of medium, K
U_i	—	Tangential speed, m s^{-1}
V_i	—	Partial molar volume, $\text{m}^3 \text{mol}^{-1}$
V	—	Cumulative filtered volume, m^3
V_i	—	Partial molar volume of i , $\text{m}^3 \text{mol}^{-1}$
v_i	—	Elementary filtered volume, m^3
x	—	Filtration length, m
z	—	Effective membrane thickness, m

Greek

α	—	Hydraulic cake resistance, m/Kg
β	—	Dimensionless recovery rate of the membrane
ΔP_m	—	Transmembrane pressure, Pa
$\Delta P_m/P_p$	—	Pressure report
$\Delta \pi$	—	osmotic pressure, kPa
λ	—	Charge lost singular and linear
γ	—	Surface global energy, N/m
μ_i	—	Chemical potential, J mol^{-1}
μ	—	Dynamic velocity of solvent, Pa s
Ψ	—	Characteristic size
ε	—	Membrane porosity
τ	—	Tortuosity factor

Acronyms

Al_2O_3	—	Aluminum oxide membrane
CFS–MFI	—	Cross-flow sampler–modified fouling index
$\text{MFI}_{0.45}$	—	Modified fouling index for membrane diameter $0.45 \mu\text{m}$
MFI–UFT	—	Modified fouling index–tangential ultrafiltration
NFT	—	Tangential nanofiltration
Adjusted R^2	—	Correlation coefficient for the correct point value
Sum of squares	—	Variance of experimental volume value
TiO_2	—	Titan oxide membrane

UFT	–	Tangential ultrafiltration
ZrO ₂	–	Zircon oxide membrane
ZnO	–	Zinc oxide

References

- [1] P. Bacchin., M. Meireles, P. Aimar, Modelling of filtration: from the polarised layer to deposit formation and compaction, *Desalination*, 145 (2002) 139–146.
- [2] H. Li, H. Xia, Y. Mei, Modeling organic fouling of reverse osmosis membrane: from adsorption to fouling layer formation, *Desalination*, 386 (2016) 25–31.
- [3] S. Judd, Principles and Applications of Membrane Bioreactors in Water and Wastewater Treatment, 1st ed., Elsevier, UK, 2006.
- [4] B. Ozdemir, A. Saatci, O. Yenigun, Evaluation of cake filtration biological reactors (CFBR) vs. membrane biological reactors (MBR) in a pilot scale plant, *Desalination*, 288 (2012) 135–144.
- [5] P. Bacchin., D. Si-Hassen, V. Starov, M.J. Clifton, P. Aimar, A unifying model for concentration polarization, gel – layer formation and particle deposition in cross-flow membrane filtration of colloidal suspensions, *Chem. Eng. Sci.*, 57 (2002) 77–91.
- [6] N. Li, J. Zhang, Y. Tian, J. Zhao, J. Zhang, W. Zuo, Anti-fouling potential evaluation of PVDF membranes modified with ZnO against polysaccharide, *Chem. Eng. J.*, 304 (2016) 165–174.
- [7] N. Li, J. Zhang, Y. Tian, J. Zhang, W. Zhan, J. Zhao, Y. Ding, W. Zuo, Hydrophilic modification of polyvinylidene fluoride membranes by ZnO atomic layer deposition using nitrogen dioxide/diethyl zinc functionalization, *J. Membr. Sci.*, 514 (2016) 241–249.
- [8] S. Khabthani, L. El-Asmi, Elementary solutions of the tangential filtration problem, 18th French Mechanical Congress, Grenoble, France, 2007.
- [9] J. Hermia, Constant pressure blocking filtration laws – application to power-law non-Newtonian fluids, *Inst. Chem. Eng.*, 60 (1982) 183–187.
- [10] J.C. Schippers, J. Verdouw, The modified fouling index, a method of determining the fouling characteristics of water, *Desalination*, 32 (1980) 137–148.
- [11] M. Shirato, M. Sambuichi, H. Kato, H. Aragaki, Internal flow mechanism in filter cakes, *AIChE J.*, 15 (1969) 405–409.
- [12] M. Pradhan, S. Vigneswaran, R. Ben Aim, J. Kandasamy, Modelling of particle deposition in a submerged membrane microfiltration system, *Desalination*, 350 (2014) 14–20.
- [13] I.O. Arukalam, E.E. Oguzie, Y. Li, Fabrication of FDTs-modified PDMS-ZnO nanocomposite hydrophobic coating with anti-fouling capability for corrosion protection of Q235 steel, *J. Colloid Interface Sci.*, 484 (2016) 220–228.
- [14] N. Maximous, G. Nakhla, K. Wong, W. Wan, Optimization of Al₂O₃/PES membranes for wastewater filtration, *Sep. Purif. Technol.*, 73 (2010) 294–301.
- [15] M. Paipuri, S.H. Kim, O. Hassan, N. Hilal, K. Morgan, Numerical modelling of concentration polarisation and cake formation in membrane filtration processes, *Desalination*, 365 (2015) 151–159.
- [16] P. Geng, G.H. Chen, Magnéli Ti₄O₇ modified ceramic membrane for electrically-assisted filtration with antifouling property, *J. Membr. Sci.*, 498 (2016) 302–314.
- [17] S. Kumar, C. Guria, A. Mandal, Synthesis, characterization and performance studies of polysulfone/bentonite nanoparticles mixed-matrix ultra-filtration membranes using oil field produced water, *Sep. Purif. Technol.*, 150 (2015) 145–158.
- [18] M. Li, Y. Zhao, S. Zhou, W. Xing, Clarification of raw rice wine by ceramic microfiltration membranes and membrane fouling analysis, *Desalination*, 256 (2010) 166–173.
- [19] C. Bouchard, J.B. Sérodes, A. Tamas, Comparative study of fouling in nanofiltration and ultrafiltration, University of Laval, Thesis.ulaval.ca / 22074, 2004, pp. 150–185.
- [20] P. Pradanos, A. Herreguez, J.I. Calvo, F. Tejerina, Mechanisms of protein fouling in cross-flow UF through an asymmetric inorganic membrane, *J. Membr. Sci.*, 114 (1996) 115–126.
- [21] X.M. Wang, X.Y. Li, A unified model for quantification of concentration polarization (CP) of particles during cross-flow membrane filtration, *Colloids Surf. A*, 407 (2012) 99–107.
- [22] Z. Changsheng, X. Jimin, R. Fen, S. Shudong, Modification of polyethersulfone membranes – a review of methods, *Prog. Mater. Sci.*, 58 (2013) 76–150.
- [23] K. Stamatakis, T. Chi, Cake formation and growth in cake filtration, *Chem. Eng. Sci.*, 46 (1991) 1917–1933.
- [24] X.M. Wang, X.Y. Li, T.D. Waite, Quantification of solid pressure in the concentration polarization (CP) layer of colloidal particles and its impact on ultrafiltration, *J. Colloid Interface Sci.*, 358 (2011) 290–300.
- [25] F. Soulié, M.S. El Yousseoufi, F. Cherblanc, C. Saix, Capillary cohesion and mechanical strength of polydisperse granular materials, *Eur. Phys. J. E*, 21 (2006) 349–357.
- [26] A. Maloberti, Membrane separation techniques: theoretical considerations, *Engineering Techniques, J.*, 2793 (2001) 2–23.
- [27] O. Kedem, A. Katchalsky, Thermodynamics analysis of the permeability of biological membranes to non-electrolytes, *Biochim. Biophys. Acta*, 27 (1958) 229–246.
- [28] Z.F. Cui., S. Chang, A.G. Fane, The use of gas bubbling to enhance membrane processes, *J. Membr. Sci.*, 221 (2003) 1–35.
- [29] P. Duran, F. Capel, C. Moure, A.R. Gonzalez-Elipse, A. Caballero, Influence of TiO₂ solid solution on the thermal property and ionic conductivity of partially stabilized zirconia, *Int. J. Appl. Ceram. Technol.*, 25 (1999) 639–648.
- [30] D.E. Smiles, P.C. Raats, J.H. Knight, Water flow in filter paper and capillary suction time, *Chem. Eng. Sci.*, 53 (1998) 2211–2218.
- [31] D.E. Smiles, Principles of Constant Pressure Filtration, N.P. Cheremisinoff, Ed., Encyclopedia of Fluid Mechanics, Vol. 5, Gulf Publishing, Houston, TX, 1986.
- [32] S.F.E. Boerlage, M.D. Kennedy, M.R. Dickson, D.E.Y. El-Hodali, J.C. Schippers, The modified fouling index using ultrafiltration membranes (MFI-UF): characterisation, filtration mechanisms and proposed reference membrane, *J. Membr. Sci.*, 197 (2002) 1–21.
- [33] L.N. Sim, Y. Ye, V. Chen, A.G. Fane, Comparison of MFI-UF constant pressure, MFI-UF constant flux and crossflow sampler-modified fouling index ultrafiltration (CFS-MFI_{UF}), *Water Res.*, 45 (2011) 1639–1650.
- [34] S. Hong, M. Elimelech, Chemical and physical aspects of natural organic matter (NOM) fouling of nanofiltration membranes, *J. Membr. Sci.*, 132 (1997) 159–181.
- [35] S.G. Salinas-Rodriguez, G.L. Amy, J.C. Schippers, M.D. Kennedy, The modified fouling index ultrafiltration constant flux for assessing particulate/colloidal fouling of RO systems, *Desalination*, 365 (2015) 79–91.
- [36] S.F.E. Boerlage, M.D. Kennedy, M.P. Aniyi, E.M. Abogrean, D.E.Y. El-Hodali, Z.S. Tarawneh, J.C. Schippers, Modified fouling index ultrafiltration to compare pretreatment processes of reverse osmosis feed water, *Desalination*, 131 (2000) 201–214.
- [37] C.H. Koo, A.W. Mohammad, M.Z.M. Talib, Setting-up of modified fouling index (MFI) and cross flow sampler – modified fouling index (CFS-MFI) measurement devices for NF/RO fouling, *J. Membr. Sci.*, 435 (2013) 165–175.
- [38] M. Elimelech, X. Zhu, A.E. Childress, S. Hong, Role of membrane surface morphology in colloidal fouling of cellulose acetate and composite aromatic polyamide reverse osmosis membranes, *J. Membr. Sci.*, 127 (1997) 101–109.
- [39] A. Jogdand, A. Chaudhuri, Modeling of concentration polarization and permeate flux variation in a roto-dynamic reverse osmosis filtration system, *Desalination*, 375 (2015) 54–70.
- [40] Z. Zhu, H. Mhemdi, Dead end ultra-filtration of sugar beet juice expressed from cold electrically pre-treated slices: effect of membrane polymer on fouling mechanism and permeate quality, *Innov. Food Sci. Emerg. Technol.*, 36 (2016) 75–82.
- [41] H. Choi, K. Zhang, D.D. Dionysiou, D.B. Oerther, G.A. Sorial, Influence of cross flow velocity on membrane performance during filtration of biological suspension, *J. Membr. Sci.*, 248 (2005) 189–199.

- [42] Y.K. Benkahla, A. Ould-Dris, M.Y. Jaffrin, D. Si-Hassen, Cake growth mechanism in cross-flow microfiltration of mineral suspensions, *J. Membr. Sci.*, 98 (1995) 107–117.
- [43] M. Hamachi, M. Mietton-Peuchot, Experimental investigations of cake characteristics in cross flow microfiltration, *Chem. Eng. Sci.*, 54 (1999) 4023–4030.
- [44] M. Hamachi, M. Cabassud, A. Davin, M. Mietton-Peuchot, Dynamic modeling of cross-flow microfiltration of bentonite suspension using recurrent neural networks, *Chem. Eng. Process.*, 38 (1999) 203–210.
- [45] Y. Marselina, P. Le-Clech, R. Stuetz, V. Chen, Detailed characterization of fouling deposition and removal on a hollow fiber membrane by direct observation technique, *Desalination*, 231 (2008) 3–11.
- [46] Y. Marselina, L. Lifa, P. Le-Clech, R.M. Stuetz, V. Chen, Characterization of membrane fouling deposition and removal by direct observation technique, *J. Membr. Sci.*, 341 (2009) 163–171.
- [47] X. Huang, B.G. Thomas, Modeling of transient flow phenomena in continuous casting of steel, *Can. Metall. Q.*, 37 (1998) 197–212.
- [48] S. Ergun, Fluid flow through packed columns, *Chem. Eng. Prog.*, 48 (1952) 89–94.
- [49] V.V. Tarabara, I. Koyuncu, M.R. Wiesner, Effect of hydrodynamics and solution ionic strength on permeate flux in cross-flow filtration: direct experimental observation of filter cake cross-sections, *J. Membr. Sci.*, 241 (2004) 65–78.
- [50] C. Tien, B.V. Ramarao, On analysis and modeling of cross-flow membrane filtration of particle suspensions, *Curr. Opin. Chem. Eng.*, 2 (2013) 245–254.
- [51] C. Tien, B.V. Ramarao, R. Yasarla, A blocking model of membrane filtration, *Chem. Eng. Sci.*, 111 (2014) 421–431.
- [52] R.C. Daniel, J.M. Billing, R.L. Russell, R.W. Shimskey, H.D. Smith, R.A. Peterson, Integrated pore blockage-cake filtration model for crossflow filtration, *Chem. Eng. Res. Des.*, 89 (2011) 1094–1103.
- [53] B. Lodge, S.J. Judd, A.J. Smith, Characterization of dead-end ultrafiltration of biotreated domestic wastewater, *J. Membr. Sci.*, 231 (2004) 91–98.
- [54] Y. He, P. Xu, C. Li, B. Zhang, High-concentration food wastewater treatment by an anaerobic membrane bioreactor, *Water Res.*, 39 (2005) 4110–4118.
- [55] J. Chen, M. Zhang, F. Li, L. Qian, H. Lin, L. Yang, X. Wu, X. Zhou, Y. He, B.Q. Liao, Membrane fouling in a membrane bioreactor: high filtration resistance of gel layer and its underlying mechanism, *Water Res.*, 102 (2016) 82–89.
- [56] H. Hong, M. Zhang, Y. He, J. Chen, H. Lin, Fouling mechanisms of gel layer in a submerged membrane bioreactor, *Bioresour. Technol.*, 166 (2014) 295–302.
- [57] M. Zhang, W. Peng, J. Chen, Y. He, L. Ding, A. Wang, H. Lin, H. Hong, Y. Zhang, H. Yu, A new insight into membrane fouling mechanism in submerged membrane bioreactor: osmotic pressure during cake layer filtration, *Water Res.*, 47 (2013) 2777–2786.
- [58] J. Luo, X. Hang, W. Zhai, B. Qi, W. Song, X. Chen, Y. Wan, Refining sugar cane juice by an integrated membrane process: filtration behavior of polymeric membrane at high temperature, *J. Membr. Sci.*, 509 (2016) 105–115.